



ELSEVIER

Contents lists available at ScienceDirect

Journal of Hydrology

journal homepage: www.elsevier.com/locate/jhydrol

Research papers

A daily spatially explicit stochastic rainfall generator for a semi-arid climate

Ying Zhao^{a,*}, Mark A. Nearing^b, D. Phillip Guertin^a^a School of Natural Resources and the Environment, University of Arizona, Tucson, AZ 85719, USA^b USDA-Agricultural Research Service, Southwest Watershed Research Center, Tucson, AZ 85719, USA

ARTICLE INFO

This manuscript was handled by A. Bardossy, Editor-in-Chief, with the assistance of Uwe Haberlandt, Associate Editor

Keywords:

Rainfall generator
Spatial
Semi-arid
Convective storm
Markov chain

ABSTRACT

Many semi-arid regions of the world experience rainfall patterns characterized by high spatial variability. Accurate spatial representation of different types of rainfall will facilitate the application of distributed hydrological models in these areas. This study presents a daily, spatially distributed, stochastic rainfall generator based on a first-order Markov chain model, calibrated using 50 years of rainfall observations at 88 gages from 1967 through 2016 in the 148-km² Walnut Gulch Experimental Watershed. Three types of rainfall, including convective, frontal, and tropical depression storms, were simulated separately in the generator using biweekly parameterization. Convective storms were simulated based on an elliptical shape rain cell conceptual model, whereas frontal and tropical depression storms were simulated as uniform rainfall fields over the whole watershed with introduced random variability. The rainfall generator was evaluated by comparing the mean statistics of 30 sets of 50-year simulated data versus the 50-year rain gage observed data. Most individual storm statistics and aggregated seasonal rainfall statistics were similar to the measured rainfall observations. The long-term mean values of both summer and winter rainfall amount were statistically satisfactory. This model can serve as a guide for application in areas with convective, frontal, and tropical depression storms.

1. Introduction

Precipitation is a driving force of many hydrologic processes, especially for regions with semi-arid and arid climates. However, the lack of reliable rainfall records limits the development of hydrologic research and applications. Stochastic rainfall generators can simulate the key characteristics of natural rainfall records (Wilks and Wilby, 1999). The advantage of simulated rainfall data is that they can provide long series of statistically representative records, which can be used in hydrological models, agricultural models, or climate change impact assessment to produce mathematically stable statistical representations of hydrologic response for a given weather record. As models become more sophisticated, the requirements for higher resolution and continuous rainfall series data become more important (Bonta, 2004; Breinl et al., 2017; Li et al., 2017; Serinaldi, 2009).

Rainfall has both temporal and spatial characteristics that need to be accounted for in the generation process. Point-based rainfall generators, which focus on the temporal dimension of rainfall, are the most commonly used models (Arnold and Williams, 1989; Calenda and Napolitano, 1999; Kavvas and Delleur, 1981; Papalexiou et al., 2011; Richardson, 1981; Valdes et al., 1985). These generators are based on single site observations, and therefore not designed to provide spatial

resolution. Researchers have studied the effect of spatially variable rainfall on hydrologic response. Some studies argued that the spatial variability of rainfall does not cause significant differences in runoff generation or only causes secondary effects (Beven and Hornberger, 1982; Obled et al., 1994; Schuurmans and Bierkens, 2006). These catchment sizes ranged from 71 to 287 km², which were mostly medium sized rural catchments. Obled et al. (1994) noted that their conclusions may not apply for smaller urbanized or larger rural areas. Schuurmans and Bierkens (2006) found that the spatial variability has a major effect on daily simulation of discharge, groundwater level and soil moisture, while for general longer-term behavior of the hydrological system, the areal average rainfall information is adequate. Koren et al. (1999) noted that heterogeneity of rainfall is a major factor for small scale catchments, but the fraction of the watershed covered by rainfall is not as important since rainfall is likely to cover the whole area. However, for larger scales, the fractional area of the watershed covered by rainfall is a major factor for runoff generation. Specific site conditions, in terms of either climate characteristics or size of the watershed, can lead to quite different conclusions on how spatial rainfall affects hydrological responses. In a semi-arid region, such as is found in much of the southwestern United States, where runoff is dominated by summer convective storms, transmission losses in ephemeral channels

* Corresponding author.

E-mail address: yingzhao@email.arizona.edu (Y. Zhao).

are a significant factor in the water budget (Goodrich et al., 1997; Renard et al., 1993). Thus, the spatial distribution of rainfall may matter more in these environments, creating distinctive runoff response for upper and lower streams. Bell and Moore (2000) also pointed out that convective rainfall induces more sensitivity in runoff production than does stratiform rainfall. To facilitate the accurate modeling of hydrologic response in semi-arid regions, such as in southeastern Arizona, a rainfall generator that can simulate non-uniform rainfall fields in space is needed. It will enhance the ability to apply distributed watershed hydrologic models.

Spatial rainfall generators may use multi-site data for a specific region, so they can also be referred to as multi-site rainfall generators. Compared with point-based generators, multi-site rainfall generators take spatial correlation between stations into consideration, since rainfall stations near enough are not totally independent of each other. Storms organize into groups and form linear bands or spiral bands under different weather systems in nature (Shuttleworth, 2012). In recent years there has been extensive research conducted on different types of multi-site rainfall generator models (Asong et al., 2016; Bardossy and Plate, 1992; Breinl et al., 2017; Evin et al., 2018; Ferraris et al., 2003; Leander and Buishand, 2009; Li, 2014; Mehrotra et al., 2006; Peleg and Morin, 2014; Serinaldi, 2009; Wilks, 1999). Most rainfall generators deal with two major components: rainfall occurrence and rainfall amount. There are two basic approaches for precipitation occurrence generation. One is the Richardson-type (Richardson, 1981) and the other is serial type (Racsko et al., 1991). The Richardson-type generator is based on Markov chain models, which simulates day to day rainfall occurrence using transition probabilities. Serial type generators account for long-term wet or dry trends, usually beginning with the simulation of dry and wet series of years, and then simulate rainfall amount based on dry and wet conditions.

There are also basically two types of methods for representing spatial distribution of rainfall amounts. The first type focuses on the physical structure of small scale rain cells, such as shape and size, either using rain gage data (Cowpertwait et al., 1996; Ferraris et al., 2003; Hsieh, 2002; von Hardenberg et al., 2003) or radar images to acquire the parameters (Morin et al., 2006; Peleg and Morin, 2014, 2012). The other type considers relatively larger scale rainfall fields, usually incorporating mathematical representation of the spatial correlation. Further classification of this type can include several different methods: (1) Statistical multi-site models, usually achieved by fitting empirical distributions for rainfall properties and adding spatial correlation matrix to represent inter-sites relation (Brissette et al., 2007; Khalili et al., 2009; Mehrotra and Sharma, 2007; Serinaldi, 2009; Wilks, 1998). (2) Resampling/bootstrap models, where rainfall depths were resampled from historical data (Buishand and Brandsma, 2001; Leander and Buishand, 2009). Recent improvements of resampling methods included adding a reshuffle process to maintain the spatial properties (Breinl et al., 2013, 2015). (3) Nonlinearly filtered autoregressive processes (Lanza, 2000; Mejía and Rodríguez-Iturbe, 1974; Rebora et al., 2006). (4) Generalized linear models (Asong et al., 2016; Verdin et al., 2018, 2015). (5) Fractal cascade models (Gupta and Waymire, 1993). Of all the above approaches, rain cell models are particularly appropriate to simulate convective storms, since these storms share common features of short duration and limited spatial extent (Osborn et al., 1979). Generalized linear models have failed to capture the summer convective precipitation characteristics (Verdin et al., 2015).

Rain cells can either be simulated using circular (Morin et al., 2005; Morin and Gabella, 2007; Peleg and Morin, 2014) or elliptical shapes (Barnolas et al., 2010; Peleg and Morin, 2012; Syed et al., 2003). The circular shape is easier for modeling since it only has one radius parameter, and the intensity distribution can be simplified as well because the cell is isotropic. The elliptical shape is more complex since it has both a major and minor axis, which also requires an additional

orientation parameter. It is also necessary to define the center coordinates of the cell and the coverage area for both kinds of cells. In addition to cell shape parameters, researchers also have studied the representation of rainfall intensity within the cell: (1) rain cells with a constant intensity everywhere; (2) Gaussian decay of intensity from cell center; (3) exponential decay of intensity from cell center; (4) hybrid of Gaussian and exponential decay from cell center. The use of constant intensity makes the model simpler, but not generally realistic, especially when the research focus is on sub-daily rain cell development. Féral et al. (2003) noted that the Gaussian distribution leads to a faster decay of rainfall intensity from the center outwards but to a lower gradient for the outer part. The specific function might differ from region to region, which needs further calibration based on actual data.

In this study, we will employ a Markov-chain based rain cell model to simulate daily spatial rainfall in a semi-arid watershed located in southeastern Arizona. The major objectives are: (1) present a conceptual model to characterize the spatial variation of the summer convective rainfall, (2) build a stochastic daily rainfall generator capable of simulating three types of rainfall with high spatial resolution that can be used in small to medium sized watersheds, and (3) evaluate the performance of the rainfall generator. Since temporal scale is not the primary consideration in this study, we used a daily step in this rainfall generator. The Richardson-type of generator was used for daily rainfall occurrence. The geographic area we are concerned about is dominated by convective rainfall during the summer, which is suitably represented by a rain-cell based generator. We combined simulations of individual rain cells to acquire the rainfall field over the entire watershed.

2. Methods

2.1. Study area and data

The study area is the Walnut Gulch Experimental Watershed, located in southeast Arizona, surrounding the town of Tombstone. It is a sub-watershed of the San Pedro River Basin. The USDA-ARS Southwest Research Center has been operating the watershed since the 1950s with intensive instrumentation and measurement of precipitation. The drainage area of Walnut Gulch is approximately 148 km², and elevation ranging from 1220 m to 1900 m above sea level. The average annual precipitation in this semi-arid watershed is approximately 312 mm (Goodrich et al., 2008a), following a bimodal pattern, with most precipitation occurring in summer and winter seasons (Osborn, 1983). Summer rainfall, during the months of July, August, and September, accounts for approximately 60% of the total annual amount in this region, and results from the North American Monsoon (Nichols et al., 2002; Stillman et al., 2013). The summer rain often forms as convective storms, with relatively short duration but high intensity, and cover a limited spatial extent. The spatial variation of summer convective storms is large. The winter frontal storms are, however, usually of long duration but low intensity, and usually cover the whole watershed more uniformly (Goodrich et al., 2008b; Nearing et al., 2015; Nichols et al., 2002; Stillman et al., 2013). Frontal storms during the non-summer months account for approximately 35% of the annual precipitation. Occasionally, snow occurs in winter at the watershed, but it melts quickly and does not accumulate. The remaining 5% of the annual rainfall falls in the form of tropical depression storms, usually dropping large amounts of water, much of which will be converted into runoff (Gochis et al., 2006; Osborn, 1982).

Walnut Gulch Experiment Watershed has more than sixty years of rainfall monitoring. The earliest rainfall record dates back to 1954. The current rain gage network consists of 88 digital rain gages (Fig. 1), which gives an average of approximately 0.6 gage km⁻² over the watershed. The dense network provides advantages for spatial rainfall

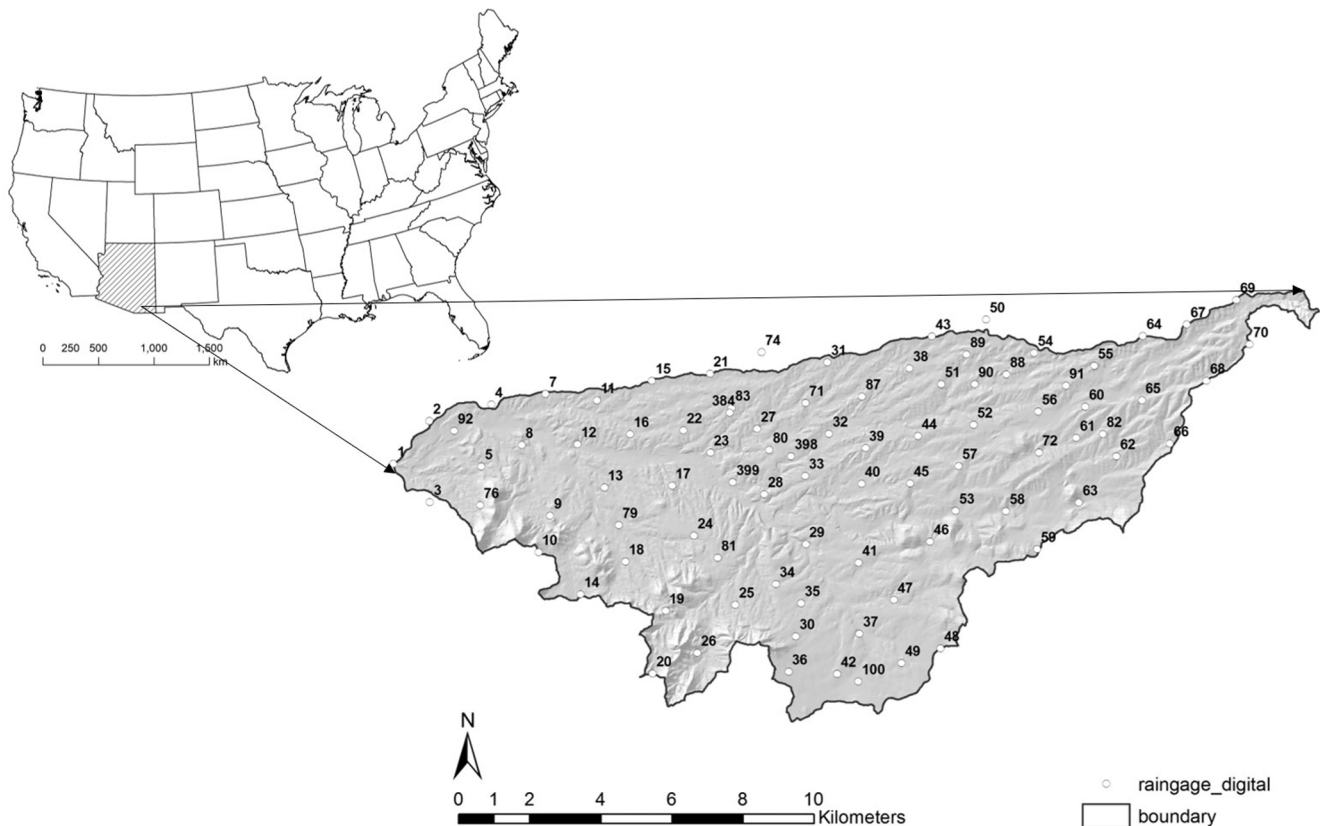


Fig. 1. Rain gage network of USDA-Agricultural Research Service Walnut Gulch Experimental Watershed, Tombstone, Arizona.

analysis, especially for the summer convective rainfall events with high spatial variation. The full current network of 88 gages was installed by 1967, so this study uses rainfall data from 1967 through 2016 (50 years) to build the generator. From 1967 through 1999, the rainfall data was recorded by analog rain gages, while after 2000, digital gages were used (Goodrich et al., 2008a). Due to resource considerations, only nine gages operated out of the monsoon season, during the winter months from 1981 through 1991 and in 1999. The reason for this is that winter rainfall in this area is much less spatially variable and the high density of rain gages were not considered necessary (Goodrich et al., 2008a). All rainfall data used can be acquired on the website of USDA-ARS-SWRC. The rainfall records are stored in an Access database, including both daily rainfall and event rainfall. The daily data recorded the year, month, day and total depth received by a certain gage on that day. The event data recorded the event ID, year, month, day, start time, duration and depth by a certain gage. Each day may have multiple events in the database for a gage. The resolution for depth is 0.254 mm (0.01 in.) and the resolution for duration is 1 min.

2.2. Storm identification

A continuous rainfall record consists of both wet periods and dry periods. Researchers have explored different methods to distinguish events, usually based on a threshold of the dry period. This threshold can be a fixed time interval for all months, such as 6 h used in erosive rainfall studies (Wischmeier and Smith, 1978). It can also vary with months, depending on the actual distribution of the inter-arrival time of rainfall in each month. The Walnut Gulch rainfall database has identified events for each gage separately and assigned an event ID to each

one. The criteria used for each gage in the database was based on a one hour hiatus (Goodrich et al., 2008a). However, this separation is only for one rain gage, which means if two gages received rainfall at the same time, they are still assigned different event IDs in the database. An actual storm occurring in the watershed usually involves more than one gage, so it is necessary to identify the individual storms within the entire gage network. According to visual perusal of daily rainfall interpolation maps (Fig. S1 in supplemental material), we determined that a reasonable storm cell number within one day was no more than five. Longer thresholds give fewer storms identified for each day, since more gage events will be combined. The 4-hour threshold to separate and identify storms was selected so that the daily storm numbers were equal to or fewer than five. When the event starting times of two gages were within that threshold, they are identified to be the same storm in the watershed. The maximum depth for each storm was also recorded during the storm identification process.

2.3. Rainfall occurrence

The rainfall generator is built with a Richardson type framework, using a first-order Markov chain model (Richardson, 1981). A flow diagram of the computational processes of rainfall generator was shown in Fig. 2. The basic concept of the first-order Markov chain method is that the present state of the system only depends on the previous state, which translated into the rainfall generation process means that the wet or dry state of the current day depends only on the state of the previous day. Using the Markov approach, a wet day is designated if at least one rain gage in the watershed receives rainfall on that day. Once a wet day is generated for the watershed, the model then generates the storm

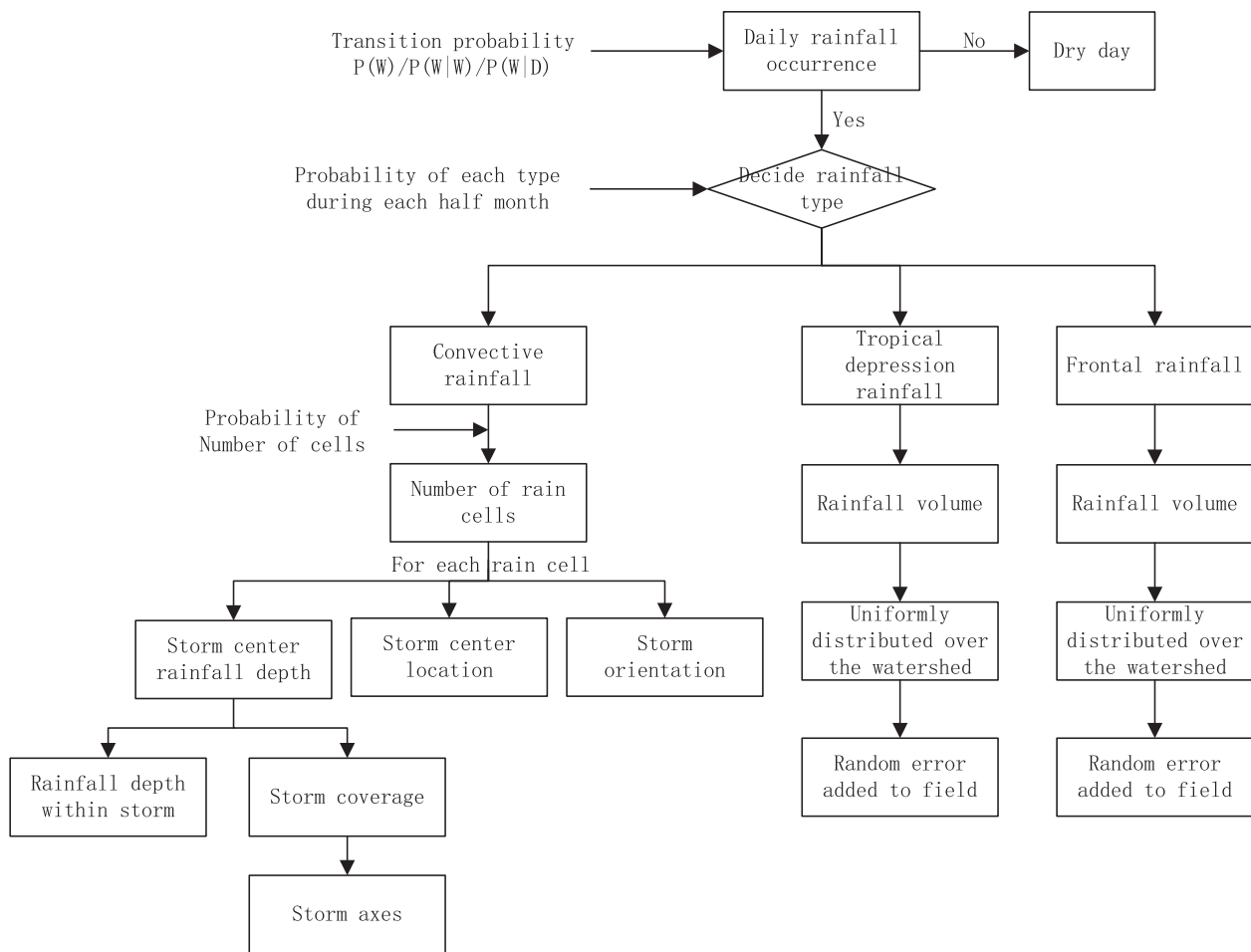


Fig. 2. Flow diagram of the computational processes in the rainfall generator.

location and coverage, which determines how much simulated rainfall each particular gage receives. In order to generate a sequence of wet and dry days, three transition probabilities need to be calculated. $P(W)$ is the probability of a wet day, $P(W|W)$ is the probability of a wet day following a wet day, and $P(W|D)$ is the probability of a wet day following a dry day. Previous research in Walnut Gulch showed that the transition probabilities for biweekly periods have significant differences from each other (Hsieh, 2002), so all transition probabilities were calculated on a biweekly basis. Modeling of the wet and dry sequence in the rainfall generator is done by first initializing a random number, and then using $P(W)$ to decide the state of first day. After the state of the previous day was decided, then the transition probabilities $P(W|W)$ and $P(W|D)$ were used to calculate the state of the next day in each biweekly period for the entire simulation sequence (Fig. 2).

When a wet day is generated, the type of rainfall also needs to be decided for that day. The consensus of most studies on Walnut Gulch is to separate each year into summer months (July–September) and non-summer months (Goodrich et al., 2008a; Nearing et al., 2015; Nichols et al., 2002; Osborn et al., 1979) in terms of differentiating rainfall types. The dominant type for summer months is convective rainfall, while the dominant type for non-summer months is frontal rainfall. The third type, tropical depression rainfall, occurs primarily in late summer and fall, from September through November (Gochis et al., 2006). Probabilities for these three types of rainfall were calculated for each biweekly period using the daily rainfall. Periods with only one type of

rainfall occurrence is straightforward, i.e. the probability of a rainfall to be a frontal type in December and January through June is 1. Similarly, the probability for convective rainfall in July through August is also 1. The complicated period is from September through November, where the probability for tropical depression storms needs to be considered. To do this, the histogram of all maximum depths of the storms in September through November were plotted, and then an exponential distribution was fitted to that histogram. The storms with large maximum depth on the histogram tails, which could not be fitted well by the exponential curve, were identified as tropical depression storms. Thus, their probabilities were calculated using the number of these storms divided by the total number of storms. All biweekly periods in September through November share the same probability of tropical depression rainfall, and the remainder of the probability for convective and frontal storms in these three months are obtained by subtracting those from 1. Thus, each day of rainfall as determined by the transition probabilities were categorized as one of the three rainfall types.

2.4. Rainfall amount and distribution

2.4.1. Convective storms

Convective storms usually show with an approximately elliptical shape in space, as determined either from interpolated daily rainfall maps or radar images (Hsieh, 2002; Karklinsky and Morin, 2006; Peleg and Morin, 2012). Hsieh (2002) analyzed convective storms in Walnut

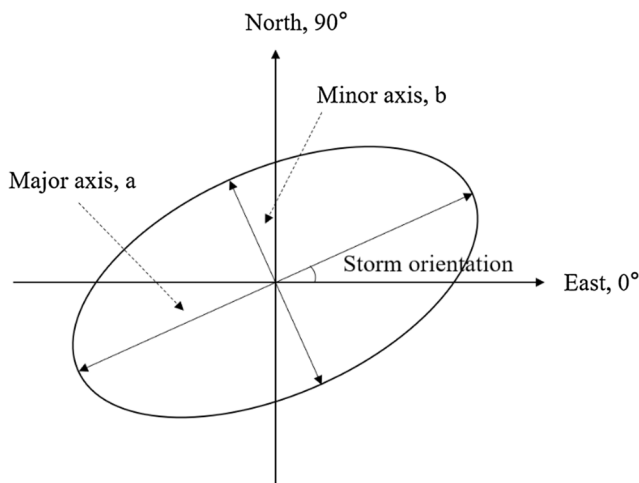


Fig. 3. Conceptual model of convective storms.

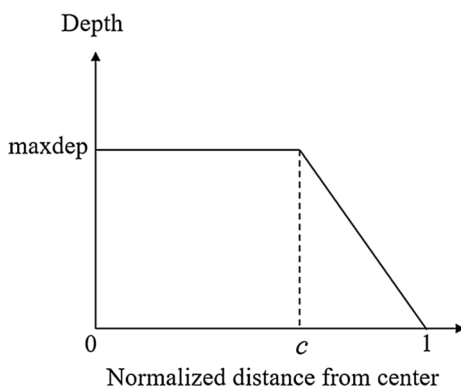


Fig. 4. Rainfall depth spread function of convective storms.

Gulch and proposed a conceptual model to characterize them (Fig. 3). This current study followed a similar conceptual model and determined several parameters using rainfall data from July through September collected in 1967 through 2016.

The previous study of Hsieh (2002) showed that the storm centers are distributed randomly in the watershed. Sometimes a storm falls only partly within the watershed boundary, which means the generated storm center can also be outside the boundary. To address this, the generator uses a slightly larger area of 26.5 km by 12.5 km, divided it into 33,125 cells, with each cell representing a 100 m by 100 m area and assigned an index from 1 through 33125. The equation to obtain a storm center location Z is:

$$z = \frac{Z}{33125} \quad (1)$$

where Z is the center index ranging from 1 through 33125, and z is the standard uniform deviate ranging from 0 to 1.

Once the storm center is located, a storm center depth is generated from a lognormal distribution and assigned to this storm. Several distributions were tested for the convective storm maximum depth, and the lognormal fit best for the data. It is assumed that the depth at the storm center is the maximum and decays to zero on the storm edge. A modified linear spread function was applied in the generator (Fig. 4), which maintains constant intensity amount around the center, and then follows a linear decay function to the edge.

$$depth = \begin{cases} max\ dep & 0 \leq r \leq c \times D \\ max\ dep(1 - r/D)/(1 - c) & c \times D < r \leq D \end{cases} \quad (2)$$

where *depth* is the rainfall depth at a certain point inside the storm extent, *max dep* is the maximum depth at storm center, *D* is the distance from the center to the edge passing through at a certain point, *r* is the distance from the center to that point, *c* is a constant between 0 and 1. The calibration of *c* was made by matching the simulated total summer rainfall amount to the observed rainfall.

The storm area is related to the maximum depth of the storm. After logarithmic transformation, a linear regression was built between the area and the maximum depth:

$$\ln(area) = a_0 + a_1 \ln(max\ dep) + \epsilon \quad (3)$$

where the units for storm area is km², and the units for maximum depth is mm, *a*₀ and *a*₁ are the coefficients of the linear regression equation, *ε* is a random error term.

An elliptical shaped storm has two axes, the major axis *a* and the minor axis *b*. The ratio *c* between them is defined as *c* = *a*/*b*. The value of *c* follows a normal distribution. Distribution parameters were acquired from Hsieh (2002). The simulated ratio was bounded between one standard deviation around the mean. When both the area and the ratio has been chosen for a storm, the length of major and minor axis can be calculated from the area equation of an ellipse.

The last parameter for a convective storm is the orientation. It is defined as the counter-clockwise angle starting from the east. The orientation for a storm is between 0 and 180 degrees and follows a normal distribution. Distribution parameters were acquired from Hsieh (2002). The simulated orientation was bounded between one standard deviation around the mean, and extreme values beyond the 0 to 180 degrees range were discarded until a new value within the range was generated.

2.4.2. Frontal storms

The frontal storms in non-summer months have much less spatial variation than do the convective storms. Osborn et al. (1979) analyzed data from Walnut Gulch in non-monsoon months, suggesting that nine gages are adequate to represent the variability of frontal storms. Rainfall interpolation maps in non-monsoon months also showed this pattern. Since frontal storms usually cover the whole Walnut Gulch, for simplicity, it is assumed that every frontal storm covers the entire watershed in the generation process. The total volume of water of each frontal storm is an important factor for quantifying annual water balance, but from a hydrologic standpoint, winter frontal storms do not generate runoff in the channels at Walnut Gulch (Goodrich et al., 2008a,b; Nearing et al., 2015).

The 88 rain gages are nearly uniformly distributed in the watershed, which means the area represented by each gage is approximately the same. The total volume of water that a storm delivers can be calculated by the following equation:

$$Vol = Dep_{avg} \times unit\ area \times N \quad (4)$$

where *Vol* is the total volume of each frontal storm, *Dep_{avg}* is the average depth of all gages receiving rainfall, *unit area* is the area of one gage represented, *N* is the number of gages receiving rainfall. Notice that the *unit area* is not a constant value throughout all the years, because with the deletion or addition of gages over time the number of gages in the full network changed during the recording period. Different *unit area* values needed to be calculated for different years. Data from 1967 through 1980, 1992 through 1998, and 2000 through 2016 were used to fit a distribution for the total volume of water per storm for each biweekly period. The extremely large values on the tails during September through November fit poorly with the overall distribution curve (Fig. S2), which indicates that they follow a different underlying

mechanism. Those storms were considered as tropical depression storms and were excluded from the dataset when building the distribution for frontal storms. The model simulation will randomly pick a storm volume from the distribution curve of each biweekly period, first spread it evenly in the whole watershed with each grid having the average depth calculated based on the volume, and then added some randomness for each grid. The random difference added to each grid is based on the standard deviations of the observed rainfall fields, and each standard deviation is corresponded to a certain average storm depth. In order to provide a reasonable variation of the generated rainfall fields, the added randomness is allowed to fluctuate between negative to positive two standard deviations.

2.4.3. Tropical depression storms

The algorithm to generate tropical depression storms is similar to that of frontal storms. The difference is that these storms are much less frequent and the volume of water dropped by this type is much larger than by frontal storms (Gochis et al., 2006; Osborn, 1982). In the previous steps, the extreme values of storm volumes in September through November were excluded and all these values were fit to a separate distribution, which was used for the tropical depression storms. Unlike the frontal storms, numbers of identified tropical depression storms were limited, so only one distribution was fit for the entire September through November period. The model simulation will randomly pick a storm volume from the distribution, first spread it evenly in the whole watershed and then add some randomness to each grid. The random difference added to each grid is based on the standard deviations of the observed rainfall fields, and each standard deviation is corresponded to a certain average storm depth. In order to provide a reasonable variation of the generated rainfall fields, the added randomness is allowed to fluctuate between negative to positive two standard deviations.

2.5. Multiple events in a day

The results in the Hsieh (2002) model underestimated the total summer rainfall of each gage, partly because the model only simulated one storm per day. Studies from radar analysis have shown that convective rainfall generally consists of several rain cells in one day (Morin et al., 2004; Peleg and Morin, 2014, 2012). Thus, the ability to simulate multiple events per day were enabled in this rainfall generator. Both convective storms and frontal storms can have multiple events per day, whereas the tropical depression storm remained as single event per day because of their sizes and durations. Based on the storm identification process in previous section, probabilities for different numbers of storms occurring in a single day may be calculated. For example, the probability of two events per day is made by counting the number of days with two storms and then dividing it by the number of total rainy days in a biweekly period. Convective rainfall would allow up to five storms per day, while frontal rainfall would allow up to three storms per day in this rainfall generator. Calibration of multiple events probabilities is based on controlling the total number of storms over the fifty-year period. For instance, if the total number of storms is overestimated, then the probability of more than one event was adjusted lower by multiplying a coefficient between 0 and 1. Consequently, probabilities for one event will be adjusted higher to maintain that the sum of all probabilities adding to one.

2.6. Statistics

Statistical analyses were performed using MATLAB. The regression equation between convective storm area and maximum depth was based on 4152 convective storms identified in 50 years, with maximum depth ranging from 0.25 mm to 95.12 mm and storm area ranging from

1.59 km² to 152.94 km². Statistical distribution types were determined for convective storm maximum depths and frontal storm and tropical depression storm volumes by comparing the empirical probability distributions to several theoretical distribution functions, such as log-normal, gamma, and exponential. The Kolmogorov–Smirnov test (K-S test) was used to test the similarity of the empirical distribution to the theoretical ones using a significance level of $\alpha = 0.05$. If more than one theoretical distribution passed the K-S test, then the one with least number of parameters was selected in further modelling processing. After the selection of distribution type, distribution parameters were fit for each type of rainfall as described previously.

2.7. Model evaluation

The rainfall generator was run for 30 sets of 50-year simulation (in total 1500 years) to obtain a sequence of simulated daily rainfall, and then compared with the observed 50 years historical rainfall data. Model performance was evaluated in two aspects: individual storm statistics and seasonally aggregated rainfall statistics. Previous research (Goodrich et al., 2008a; Nearing et al., 2015; Nichols et al., 2002) divided the year into summer months (July–September) and non-summer months (October–December, January–June), which is adopted in this study as well. The convective storm type was evaluated to determine whether the proposed conceptual model was able to capture the major storm characteristics. Seasonally aggregated rainfall amounts were evaluated based on the simulation results of six gages (Gage ID 13, 34, 44, 46, 62, 80). These gages were relatively evenly distributed inside the watershed and were selected as a sample to calculate the seasonal rainfall.

Statistics of both simulated individual storms and aggregated rainfall, including the mean, standard deviation, maximum, minimum, range and skewness, were computed and compared with the 50-year observed data. In addition, simulated and observed cumulative distribution functions (CDFs) were created for both individual storms and aggregated rainfall. K-S tests were performed between simulated and observed CDFs to determine whether they belonged to the same statistical distribution.

Time series properties were evaluated through dry and wet spell lengths of simulated and observed rainfall data. The cumulative distribution function curves of both dry and wet spells were created for summer, non-summer, and annual periods. Seasonal and annual median lengths of dry and wet spells were also calculated for comparison. K-S tests were performed between simulated and observed CDFs to determine whether they belonged to the same statistical distributions.

3. Results and discussion

3.1. Rainfall characterization

The transition probabilities for rainfall occurrence somewhere on the watershed for the 24 half-month periods are shown in Table 1. The probability of wet P(W) clearly showed that rainfall frequency reaches its peak in summer, exceeding 0.5, from the first half of July to the first half of September. The second wettest period is in winter from December through February, where P(W) ranges from 0.2 to 0.3. P(W|W) is always greater than P(W|D), which means that wet days tend to be clustered together.

Axis ratio and orientation statistics were acquired from Hsieh (2002). Those parameters were measured directly from interpolated rainfall surfaces and shown in Table 2. The mean value of axis ratio was 1.54, which is slightly greater than that found in previous work on Walnut Gulch, which showed a major to minor axis ratio of between 1.0 and 1.5 (Fogel and Duckstein, 1969). The mean value of orientation

Table 1
Transition probabilities, probabilities for three types of rainfall, and the probabilities for multiple events in all 24 half month periods.

Half month		1	2	3	4	5	6	7	8	9	10	11	12
Transition probabilities	P(W)	0.2053	0.2225	0.2547	0.1914	0.1880	0.1338	0.1147	0.0960	0.0960	0.1175	0.1240	0.2640
	P(W W)	0.4740	0.5000	0.5602	0.4776	0.4752	0.3738	0.4186	0.4167	0.3750	0.5106	0.4624	0.6111
	P(W D)	0.1359	0.1431	0.1503	0.1237	0.1215	0.0952	0.0753	0.0619	0.0664	0.0652	0.0761	0.1377
Probabilities for types of rainfall	Convective	0	0	0	0	0	0	0	0	0	0	0	0
	Frontal	1	1	1	1	1	1	1	1	1	1	1	1
	Tropical	0	0	0	0	0	0	0	0	0	0	0	0
Probabilities for multiple events	1	0.7309	0.7155	0.6589	0.7629	0.6751	0.7312	0.6690	0.8808	0.8217	0.7066	0.7868	0.8031
	2	0.1651	0.1626	0.2321	0.1626	0.2188	0.1680	0.2242	0.1022	0.1426	0.1726	0.1745	0.1663
	3	0.1040	0.1219	0.1089	0.0745	0.1061	0.1008	0.1068	0.0170	0.0357	0.1208	0.0388	0.0306
	4												
	5												
Parameter of distributions*	μ (mm or 10^5 m^3)	2.6923	2.8794	2.1721	1.8628	2.6981	2.0318	1.5667	1.6052	1.4837	1.6541	2.3326	2.1434
	σ (mm)												

Half month		13	14	15	16	17	18	19	20	21	22	23	24
Transition probabilities	P(W)	0.6213	0.7738	0.7547	0.6438	0.5320	0.2733	0.2160	0.1950	0.1440	0.1613	0.2173	0.2288
	P(W W)	0.7854	0.8336	0.8269	0.7592	0.7118	0.5561	0.5185	0.4615	0.4444	0.3884	0.5215	0.5191
	P(W D)	0.3521	0.5635	0.5326	0.4316	0.3276	0.1651	0.1327	0.1304	0.0935	0.1176	0.1329	0.1410
Probabilities for types of rainfall	Convective	1	1	1	1	0.9876	0.9876	0	0	0	0	0	0
	Frontal	0	0	0	0	0	0	0.9876	0.9876	0.9876	0.9876	1	1
	Tropical	0	0	0	0	0.0124	0.0124	0.0124	0.0124	0.0124	0.0124	0	0
Probabilities for multiple events	1	0.6449	0.6499	0.6450	0.6842	0.7133	0.6966	0.7409	0.7515	0.7496	0.7596	0.7801	0.6929
	2	0.2187	0.2227	0.2171	0.2178	0.1633	0.1678	0.1766	0.1792	0.2019	0.1492	0.1367	0.1906
	3	0.0961	0.0911	0.0953	0.0713	0.0867	0.0807	0.0824	0.0694	0.0485	0.0912	0.0832	0.1165
	4	0.0362	0.0300	0.0310	0.0255	0.0250	0.0323						
	5	0.0042	0.0062	0.0115	0.0013	0.0117	0.0226						
Parameter of distributions*	μ (mm or 10^5 m^3)	1.5314	1.7461	1.6551	1.6105	1.6272	1.3189	2.4079	2.4877	2.5405	2.0375	3.2548	2.3647
	σ (mm)	1.4235	1.4680	1.4851	1.4827	1.4576	1.5344						

* (1) July–September (13–18): lognormal distribution for convective rainfall maximum depth, unit: mm. (2) Other months (1–12, 19–24): exponential distribution for frontal rainfall volume, unit: 10^5 m^3 . (3) September–November (17–22): μ of exponential distribution for tropical depression rainfall is $4.2643 \times 10^6 \text{ m}^3$.

Table 2
Characteristics of convective storm area, axis ratio, and orientation.

	Mean	Std. dev.	Skewness	Max	Min
Area (km^2)	58.01	50.50	0.56	152.94	1.59
Axis ratio (a/b)*	1.54	0.37	0.96	2.50	1.08
Orientation (degree)*	91.40	38.27	0.06	170.00	0.00

*From Hsieh (2002).

found in Hsieh (2002) was 91.40, which points generally north as defined in the previous section. The area statistics acquired in this study showed a mean of 58.01 km^2 , which is approximately one-third of the watershed area. The regression equation of area and maximum depth (see Eq. (3)) was determined as:

$$\ln(\text{area}) = 2.1784 + 0.6851 \ln(\text{max dep}) + \varepsilon \quad (R^2 = 0.57, n = 4152) \quad (5)$$

Hsieh (2002), using data also from Walnut Gulch, developed a similar regression equation (Eq. (6)) between area and maximum depth from 48 interpolated storm surfaces, with the maximum depth ranging from 4.83 mm to 47.75 mm, and storm areas ranging from 3.6 km^2 to 181.26 km^2 .

$$\ln(\text{area}) = 1.1569 + 0.93 \ln(\text{max dep}) + \varepsilon \quad (R^2 = 0.46, n = 48) \quad (6)$$

The number of storms used in this study was much greater than used by Hsieh (2002). The slope of Eq. (5) is less than Eq. (6), because the 48 storm samples Hsieh chose were mostly larger storms with clear elliptical shapes in space, which may be biased in terms of area

representation.

The decay function to distribute rainfall from the convective storm center to the edge was determined as (see Fig. 4):

$$\text{depth} = \begin{cases} \text{max dep} & 0 \leq r \leq 0.59D \\ \text{maxdep}(1 - r/D)/0.41 & 0.59D < r \leq D \end{cases} \quad (7)$$

Previous work on Walnut Gulch has used either an exponential type decay function (Fogel and Duckstein, 1969) or simple linear decay function (Hsieh, 2002) to distribute the rainfall from the storm center to the edge. However, in this study, we found that these two methods both underestimate the rainfall total. Observed from radar images and interpolated rain gage isohyets, the convective rain cell tends to have a flat distribution around the center. The rationale behind it is that as the storm moves in space it creates a region with relatively uniform maximum depth in the storm center (Fogel and Duckstein, 1969).

Other model parameters, including the probabilities for different types of rainfall, probabilities for multiple events occurring in a day, and the distribution parameters for rainfall amount are shown in Table 1. The distribution for convective storm maximum depth was determined to be lognormal with two parameters, mean (μ) and variance (σ), the fitting plots were shown in supplemental material Fig. S3. Whereas, the best-fit distribution for frontal and tropical depression storms was determined to be exponential, with only one parameter μ , and fitting plots were shown in supplemental material Fig. S4. Notice that the units for convective storms and the other two types are different in Table 1, because one is for depth and the other two are for volume.

Table 3
 Characteristics of convective storm maximum depths (mm).

	Observed						Simulated					
	July 1–15	July 16–31	Aug 1–15	Aug 16–31	Sept 1–15	Sept 16–30	July 1–15	July 16–31	Aug 1–15	Aug 16–31	Sept 1–15	Sept 16–30
Mean	10.32	12.85	12.05	11.52	11.38	9.45	10.26	13.23	12.73	11.73	11.93	9.46
Std. dev.	12.62	14.78	14.30	13.58	13.41	12.99	14.86	20.08	19.36	17.53	17.85	14.94
Max	85.60	83.31	91.19	81.03	87.63	95.12	104.28	143.36	136.68	129.45	125.26	108.26
Min	0.25	0.25	0.25	0.25	0.25	0.25	0.25	0.25	0.25	0.25	0.25	0.25
Range	85.34	83.06	90.93	80.77	87.38	94.87	104.03	143.11	136.43	129.20	125.01	108.01
Skewness	2.25	1.79	1.91	1.86	2.03	2.85	2.97	3.07	3.05	3.01	3.05	3.25

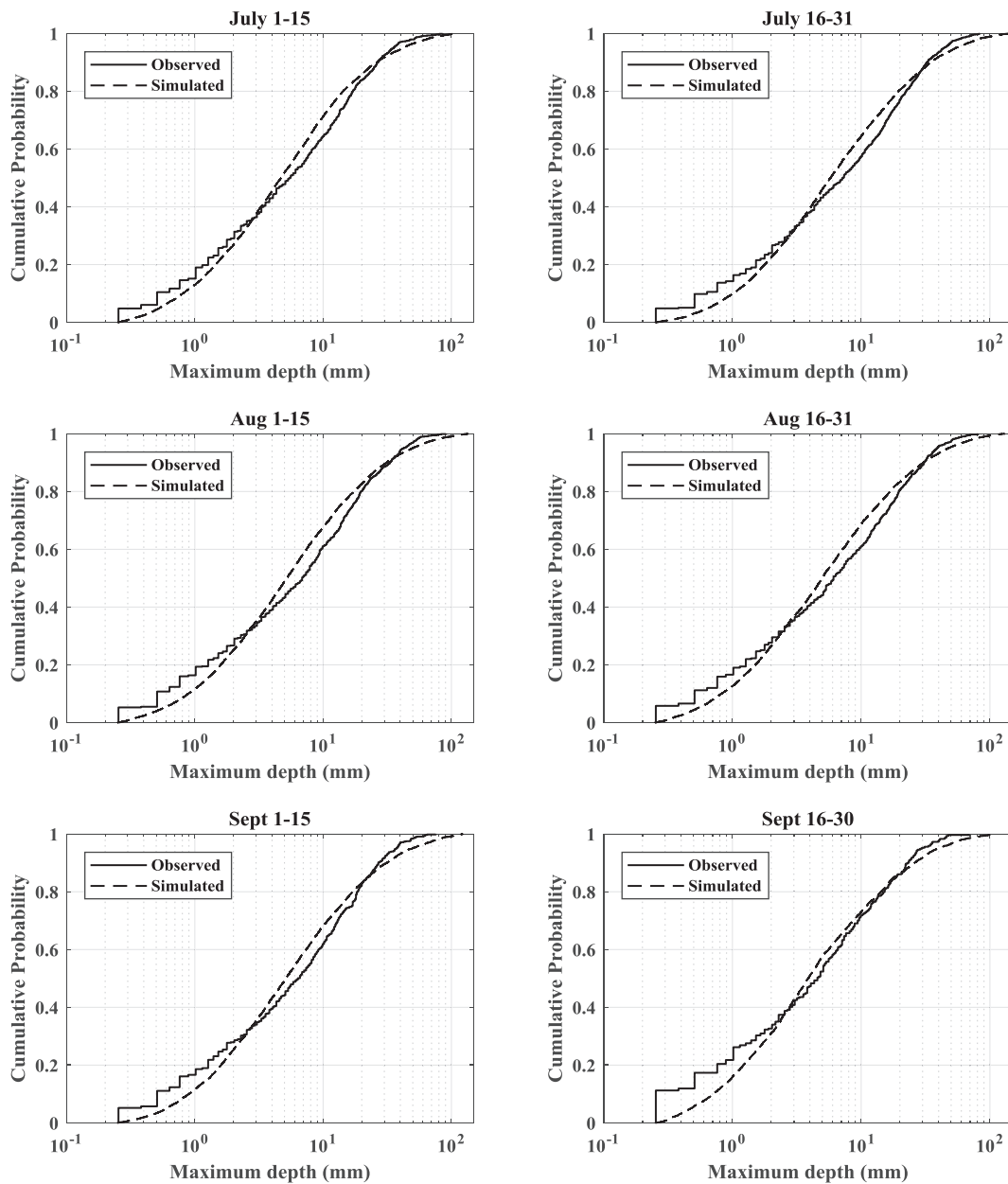


Fig. 5. CDFs of observed and simulated summer convective storm maximum depths.

Table 4
Observed and simulated rainfall totals for summer months of six gages (mm).

Gage ID	Observed						Simulated					
	13	34	44	46	62	80	13	34	44	46	62	80
Mean	186.7	192.2	194.6	199.5	194.5	189.7	196.3	187.1	185.8	191.8	186.5	195.0
Std. dev.	60.4	63.7	58.6	61.4	52.2	66.8	100.4	99.7	101.6	102.6	96.3	100.7
Max	336.6	345.7	345.9	410.5	327.3	380.0	508.3	561.7	623.5	617.3	534.2	511.9
Min	89.8	70.2	81.0	77.7	88.8	75.4	3.6	1.5	7.2	8.2	10.4	9.1
Range	246.8	275.5	264.9	332.7	238.5	304.5	504.8	560.2	616.3	609.1	523.9	502.8
Skewness	0.5	0.4	0.4	0.5	-0.2	0.6	0.5	0.6	1.0	0.9	0.6	0.6

3.2. Model evaluation

The statistics of observed and simulated convective storm maximum depth from July through September are presented in Table 3. The mean value simulated in all six half months with convective storms had less than 6% difference. The fact that the simulated storm depths had a broader range of maximum depths is expected since the model was run for 30 sets of 50-year time range (in total 1500 years) and should include extreme values that were not captured in the historical data. The shape of simulated and observed CDF curves for all six periods were similar (Fig. 5). The K-S test showed that there were no significant ($\alpha = 0.05$) differences between the observed and simulated CDFs in all half month periods.

The average summer rainfall total of the selected six gages was 192.9 mm, whereas the simulated summer rainfall total was 190.4 mm, with 1.3% difference (Table 4). The simulated range of summer rainfall total was almost twice that of the observed values, with lesser minimum and greater maximum values. Consequently, the simulated standard deviation was approximately 100 mm, which was greater than the observed values which were approximately 60 mm. K-S test results showed that there was no significant difference between the two curves in summer (Fig. 6a), under $\alpha = 0.05$ significance level. The simulated data variability was greater than the historical data, could have resulted from more extreme values being simulated in the long synthetic time series. This is consistent with the individual convective storms evaluation, where some extreme values exceeding the historical records were simulated.

As for non-summer rainfall, observed mean of six gages was 122.6 mm, and the simulated mean was 122.2 mm (Table 5). The range of winter rainfall had 15.6% difference between the observed and simulated, which is mostly caused by the overestimation of the minimum values. The simulated maximum winter rainfall was slightly less than the observed. Thus, the standard deviation was also underestimated by the model compared to historical records. The reason for this is related to the method used to distribute the generated the rainfall volume over

the watershed. Since winter frontal storms have less variability than summer convective rainfall, for simplicity in this rainfall generator, every storm volume was distributed uniformly to all gages, only adding a small random variance. As a result, the variation in both space and time has been lost to some degree. The two CDF curves of non-summer rainfall total amounts failed the K-S test (Fig. 6b), which means that there was some difference between the simulated and observed data. However, the winter storms in Walnut Gulch rarely cause runoff and erosion due to their low intensity (Goodrich et al., 2008a,b; Nearing et al., 2015), so it was considered acceptable to miss some variation in the generated storm depth totals as long as the mean total amount is similar and annual water balance is maintained.

Simulated and observed median lengths of dry and wet spell were shown in Table 6, which represents the central tendency of spell length distribution. The median of simulated dry spell length was slightly shorter than observed throughout the year, whereas the median of simulated wet spell length was longer than observed for summer, but the same for non-summer months. The overestimated wet spell length also caused an overestimation for annual wet spell length. The cumulative distribution function curves for seasonal and annual were shown in Fig. 7. Five of the six pairs of observed and simulated curves passed the K-S test under $\alpha = 0.05$ significance level. The significant difference for the summer wet spell curves indicated that the rainfall generator tends to simulate slightly longer wet periods during summer season.

4. Conclusion

This study presented modeling concepts and processes of a daily, spatial, stochastic rainfall generator in a semi-arid watershed in southeastern Arizona. Unlike most daily rainfall generators which give only the daily rainfall amount, this model is capable of simulating individual storms within a day. Simulation of four elements, including daily rainfall occurrence, the number of storms per day, the maximum depth or total volume of a storm, and spatial distribution of the rainfall was illustrated using 50-years of rain gage observations in Walnut

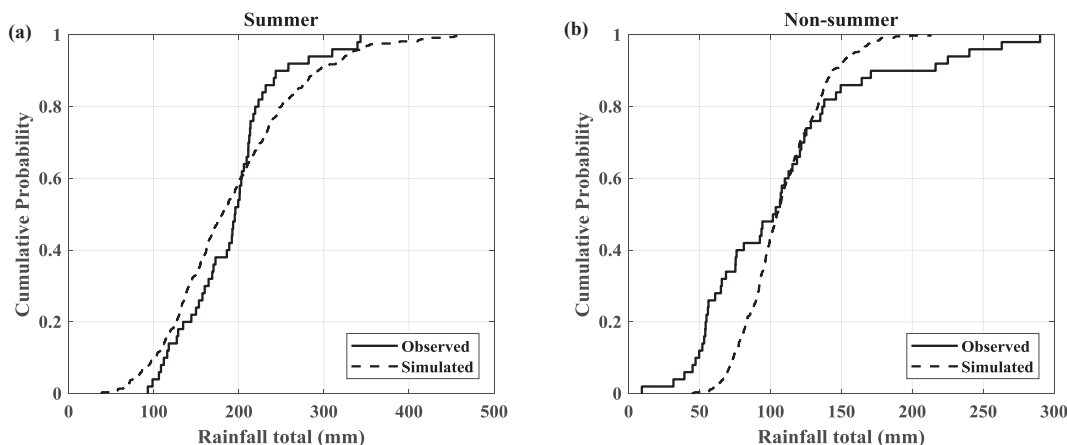


Fig. 6. CDFs of observed and simulated rainfall totals for (a) summer and (b) non-summer periods.

Table 5
Observed and simulated rainfall totals for non-summer months of six gages (mm).

Gage ID	Observed						Simulated					
	13	34	44	46	62	80	13	34	44	46	62	80
Mean	122.7	120.7	121.6	132.8	116.9	120.9	122.6	122.0	122.0	122.7	121.6	122.1
Std. dev.	59.7	65.8	61.1	65.1	64.3	59.8	34.2	34.1	33.7	34.7	34.0	34.3
Max	266.4	308.9	295.0	318.8	300.4	282.8	265.0	305.8	282.0	280.8	264.7	256.8
Min	19.8	18.0	13.2	16.3	10.7	12.2	42.3	41.9	42.3	33.2	44.7	30.3
Range	246.6	290.8	281.8	302.5	289.7	270.6	222.7	263.9	239.8	247.6	219.9	226.5
Skewness	0.6	0.9	0.9	0.8	1.2	0.7	0.5	0.6	0.4	0.5	0.6	0.4

Table 6
Observed and simulated median length of dry and wet spells (day).

	Observed			Simulated			
	Annual	Summer	Non-summer	Annual	Summer	Non-summer	
Dry_observed	4.2	2.2	7.2	Wet_observed	1.0	1.0	1.0
Dry_simulated	4.0	2.0	6.0	Wet_simulated	2.0	3.0	1.0

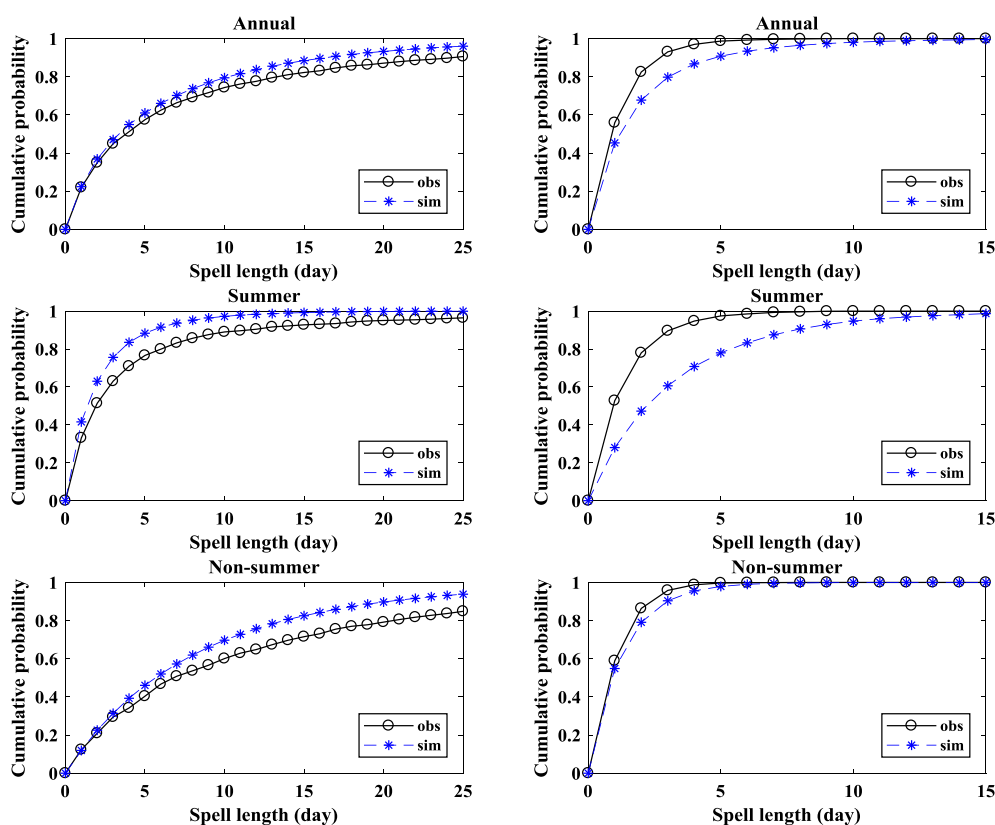


Fig. 7. CDFs of observed and simulated dry and wet spell length for annual, summer and non-summer periods, (1) first column: dry spell, (2) second column: wet spell.

Gulch Experimental Watershed, Arizona. The separation process of generating three types of rainfall (convective, frontal and tropical depression) is appropriate in this region, since they all have quite different physical features. The concept of elliptical shape of convective storms works well in this study and has been tested in other research. The simulated individual convective storm statistics were similar to the observed. The simulated seasonal rainfall performed differently for summer and non-summer periods, with a slight overestimation of variation of annual summer rainfall and an underestimation of variation in

non-summer period, but the long-term mean values of both summer and non-summer periods are satisfactory.

There are limitations for this generator. It is a well calibrated model based on the dense rain gage network of Walnut Gulch Experimental Watershed, and expanding it to larger area application will require additional analysis linking the point statistics with area statistics. Possible solutions for obtaining larger area statistics, such as convective storm area, may need incorporation of radar rainfall images. This rainfall generator is initially targeted at semi-arid watersheds where

convective rainfall dominated, thus it may not be immediately applicable in regions with significantly different rainfall types.

Possible uses of the rainfall generator include application into hydrological models, erosion models as rainfall input, where spatial rainfall information could have an impact on runoff response or sediment yield. It may also be applied in climate change studies by manipulating model parameters to account for future trends and testing the outcomes. Developing the rainfall generator into a high-resolution temporal model is a future research need, which will require further studies of storm movement in space and time.

Acknowledgements

Acknowledgement goes to the field staff of the Walnut Gulch Experimental Watershed and all of the previous scientists and staff of the USDA-ARS Southwest Watershed Research Center for the dedication and effort that made the collection and use of these data possible. Rainfall data used in this study can be acquired at <http://www.tucson.ars.ag.gov/dap/>.

This work was funded by a Specific Cooperative Agreement between the USDA Agricultural Research Service (Agreement number 58-53424-018) and the University of Arizona (Agreement number 2022-13610-012-22S).

Declarations of interest

The authors declare that they have no known competing financial interests or personal relationships that could have appeared to influence the work reported in this paper.

Appendix A. Supplementary data

Supplementary data to this article can be found online at <https://doi.org/10.1016/j.jhydrol.2019.04.006>.

References

- Arnold, J.G., Williams, J.R., 1989. Stochastic generation of internal storm structure at a point. *Trans. ASAE* 32, 161–167.
- Asong, Z.E., Khalil, M.N., Wheat, H.S., 2016. Multisite multivariate modeling of daily precipitation and temperature in the Canadian Prairie Provinces using generalized linear models. *Clim. Dyn.* 47, 1–21. <https://doi.org/10.1007/s00382-016-3004-z>.
- Bardossy, A., Plate, E.J., 1992. Space-time model for daily rainfall using atmospheric circula.pdf.
- Barnolas, M., Rigo, T., Llasat, M.C., 2010. Characteristics of 2-D convective structures in Catalonia (NE Spain): an analysis using radar data and GIS. *Hydrol. Earth Syst. Sci.* 14, 129–139. <https://doi.org/10.1016/j.atmosres.2005.08.014>.
- Bell, V.A., Moore, R.J., 2000. The sensitivity of catchment runoff models to rainfall data at different spatial scales. *Hydrol. Earth Syst. Sci.* <https://doi.org/10.5194/hess-4-653-2000>.
- Beven, K., Hornberger, G., 1982. Assessing the effect of spatial pattern of precipitation in modeling stream flow hydrographs. *Water Resour. Bull.* 18, 823–829. <https://doi.org/10.1111/j.1752-1688.1982.tb00078.x>.
- Bonta, J.V., 2004. Stochastic simulation of storm occurrence, depth, duration and within-storm intensities. *Trans. ASAE* 47, 1573–1584.
- Breini, K., Di Baldassarre, G., Giron Lopez, M., Hagenlocher, M., Vico, G., Rutgersson, A., 2017. Can weather generation capture precipitation patterns across different climates, spatial scales and under data scarcity? *Sci. Rep.* 7, 3–7. <https://doi.org/10.1038/s41598-017-05822-y>.
- Breini, K., Turkington, T., Stowasser, M., 2015. Simulating daily precipitation and temperature: a weather generation framework for assessing hydrometeorological hazards. *Meteorol. Appl.* 22, 334–347. <https://doi.org/10.1002/met.1459>.
- Breini, K., Turkington, T., Stowasser, M., 2013. Stochastic generation of multi-site daily precipitation for applications in risk management. *J. Hydrol.* 498, 23–35. <https://doi.org/10.1016/j.jhydrol.2013.06.015>.
- Brissette, F.P., Khalil, M., Leconte, R., 2007. Efficient stochastic generation of multi-site synthetic precipitation data. *J. Hydrol.* 345, 121–133. <https://doi.org/10.1016/j.jhydrol.2007.06.035>.
- Buishand, T.A., Brandsma, T., 2001. Multisite simulation of daily precipitation and temperature in the Rhine basin by nearest-neighbor resampling. *Water Resour. Res.* 37, 2761–2776. <https://doi.org/10.1029/2001WR000291>.
- Calenda, G., Napolitano, F., 1999. Parameter estimation of Neyman-Scott processes for temporal point rainfall simulation. *J. Hydrol.* 225, 45–66. [https://doi.org/10.1016/S0022-1694\(99\)00133-X](https://doi.org/10.1016/S0022-1694(99)00133-X).
- Cowpertwait, P.S.P., O'Connell, P.E., Metcalfe, A.V., Mawdsley, J.A., 1996. Stochastic point process modelling of rainfall. II. Regionalisation and disaggregation. *J. Hydrol.* 175, 47–65. [https://doi.org/10.1016/S0022-1694\(96\)80005-9](https://doi.org/10.1016/S0022-1694(96)80005-9).
- Evin, G., Favre, A.C., Hingray, B., 2018. Stochastic generation of multi-site daily precipitation focusing on extreme events. *Hydrol. Earth Syst. Sci.* 22, 655–672. <https://doi.org/10.5194/hess-22-655-2018>.
- Féral, L., Sauvageot, H., Castanet, L., Lemorton, J., 2003. HYCELL – a new hybrid model of the rain horizontal distribution for propagation studies: 1. Modeling of the rain cell. *Radio Sci.* 38, 1–20. <https://doi.org/10.1029/2002RS002802>.
- Ferraris, L., Gabellani, S., Rebora, N., Provenzale, A., 2003. A comparison of stochastic models for spatial rainfall downscaling. *Water Resour. Res.* 39, 1–8. <https://doi.org/10.1029/2003WR002504>.
- Fogel, M.M., Duckstein, L., 1969. Point rainfall frequencies in convective storms. *Water Resour. Res.* 5, 1229–1237. <https://doi.org/10.1029/WR005i006p01229>.
- Gochis, D.J., Brito-Castillo, L., Shuttleworth, W.J., 2006. Hydroclimatology of the North American Monsoon region in northwest Mexico. *J. Hydrol.* 316, 53–70. <https://doi.org/10.1016/j.jhydrol.2005.04.021>.
- Goodrich, D.C., Keefer, T.O., Unkrich, C.L., Nichols, M.H., Osborn, H.B., Stone, J.J., Smith, J.R., 2008a. Long-term precipitation database, Walnut Gulch Experimental Watershed, Arizona, United States. *Water Resour. Res.* 44, W05S04. <https://doi.org/10.1029/2006WR005782>.
- Goodrich, D.C., Lane, L.J., Shillito, R.M., Miller, S.N., Syed, K.H., Woolhiser, A., 1997. Linearity of basin response as a function of scale in a semiarid watershed. *Water Resour. Res.* 33, 2951–2965.
- Goodrich, D.C., Unkrich, C.L., Keefer, T.O., Nichols, M.H., Stone, J.J., Levick, L.R., Scott, R.L., 2008b. Event to multidecadal persistence in rainfall and runoff in southeast Arizona. *Water Resour. Res.* 44, W05S14. <https://doi.org/10.1029/2007WR006222>.
- Gupta, V.K., Waymire, E.C., 1993. A Statistical analysis of mesoscale rainfall as a random cascade. *J. Appl. Meteorol.* 32, 251–267. [https://doi.org/10.1175/1520-0450\(1993\)032<0251:ASAOMR>2.0.CO;2](https://doi.org/10.1175/1520-0450(1993)032<0251:ASAOMR>2.0.CO;2).
- Hsieh, H.-H., 2002. Stochastic Daily Thunderstorm Generation in Southeast Arizona. *Univ. Arizona* <https://doi.org/10.16953/deusbed.74839>.
- Karklinsky, M., Morin, E., 2006. Spatial characteristics of radar-derived convective rain cells over southern Israel. *Meteorol. Zeitschrift* 15, 513–520. <https://doi.org/10.1127/0941-2948/2006/0153>.
- Kavvas, L., Delleur, J.W., 1981. Cluster model of daily rainfall sequences. *Water Resour. Res.* 17, 1151–1160. <https://doi.org/10.1029/WR017i004p01151>.
- Khalili, M., Brissette, F., Leconte, R., 2009. Stochastic multi-site generation of daily weather data. *Stoch. Environ. Res. Risk Assess.* 23, 837–849. <https://doi.org/10.1007/s00477-008-0275-x>.
- Koren, V.I., Finnerty, B.D., Schaake, J.C., Smith, M.B., Seo, D.J., Duan, Q.Y., 1999. Scale dependencies of hydrologic models to spatial variability of precipitation. *J. Hydrol.* 217, 285–302. [https://doi.org/10.1016/S0022-1694\(98\)00231-5](https://doi.org/10.1016/S0022-1694(98)00231-5).
- Lanza, L.G., 2000. A conditional simulation model of intermittent rain fields. *Hydrol. Earth Syst. Sci.* <https://doi.org/10.5194/hess-4-173-2000>.
- Leander, R., Buishand, T.A., 2009. A daily weather generator based on a two-stage resampling algorithm. *J. Hydrol.* 374, 185–195. <https://doi.org/10.1016/j.jhydrol.2009.06.010>.
- Li, Z., 2014. A new framework for multi-site weather generator: a two-stage model combining a parametric method with a distribution-free shuffle procedure. *Clim. Dyn.* 43, 657–669. <https://doi.org/10.1007/s00382-013-1979-2>.
- Li, Z., Lü, Z., Li, J., Shi, X., 2017. Links between the spatial structure of weather generator and hydrological modeling. *Theor. Appl. Climatol.* 128, 103–111. <https://doi.org/10.1007/s00704-015-1691-8>.
- Mehrotra, R., Sharma, A., 2007. A semi-parametric model for stochastic generation of multi-site daily rainfall exhibiting low-frequency variability. *J. Hydrol.* 335, 180–193. <https://doi.org/10.1016/j.jhydrol.2006.11.011>.
- Mehrotra, R., Srikanthan, R., Sharma, A., 2006. A comparison of three stochastic multi-site precipitation occurrence generators. *J. Hydrol.* 331, 280–292. <https://doi.org/10.1016/j.jhydrol.2006.05.016>.
- Mejía, J.M., Rodríguez-Iturbe, I., 1974. On the synthesis of random field sampling from the spectrum: an application to the generation of hydrologic spatial processes. *Water Resour. Res.* 10 (4), 705–711. <https://doi.org/10.1029/WR010i004p00705>.
- Morin, E., Gabella, M., 2007. Radar-based quantitative precipitation estimation over Mediterranean and dry climate regimes. *J. Geophys. Res. Atmos.* 112, 1–13. <https://doi.org/10.1029/2006JD008206>.
- Morin, E., Goodrich, D., Maddox, R., Gao, X., Gupta, H., 2004. Spatial patterns in thunderstorm rainfall events: conceptual modeling and hydrological insights. *Sixth International Symposium on Hydrological Applications of Weather Radar*.
- Morin, E., Goodrich, D.C., Maddox, R.A., Gao, X., Gupta, H.V., Sorooshian, S., 2006. Spatial patterns in thunderstorm rainfall events and their coupling with watershed hydrological response. *Adv. Water Resour.* 29, 843–860. <https://doi.org/10.1016/j.advwatres.2005.07.014>.
- Morin, E., Goodrich, D.C., Maddox, R.A., Gao, X., Gupta, H.V., Sorooshian, S., 2005. Rainfall modeling for integrating radar information into hydrological model. *Atmos. Sci. Lett.* 6, 23–30. <https://doi.org/10.1002/asl.86>.
- Nearing, M.A., Unkrich, C.L., Goodrich, D.C., Nichols, M.H., Keefer, T.O., 2015. Temporal and elevation trends in rainfall erosivity on a 149 km² watershed in a semi-arid region of the American Southwest. *Int. Soil Water Conserv. Res.* 3, 77–85. <https://doi.org/10.1016/j.iswcr.2015.06.008>.
- Nichols, M.H., Renard, K.G., Osborn, H.B., 2002. Precipitation changes from 1956 to 1996 on the Walnut Gulch Experimental Watershed. *J. Am. Water Resour. Assoc.* 38, 161–172. <https://doi.org/10.1111/j.1752-1688.2002.tb01543.x>.
- Obled, C., Wendling, J., Beven, K., 1994. The sensitivity of hydrological models to spatial rainfall patterns: an evaluation using observed data. *J. Hydrol.* 159, 305–333. [https://doi.org/10.1016/0022-1694\(94\)90263-1](https://doi.org/10.1016/0022-1694(94)90263-1).

- Osborn, H.B., 1983. Precipitation Characteristics Affecting Hydrologic Response of Southwestern Rangelands. Agricultural Research Service Agricultural Reviews and Manuals, Western Series, No. 34.
- Osborn, H.B., 1982. Quantifiable differences between airmass and frontal-convective thunderstorm rainfall in the southwestern United States. In: *Statistical Analysis of Rainfall and Runoff*, pp. 21–32.
- Osborn, H.B., Renard, K.G., Simanton, J.R., 1979. Dense networks to measure convective rainfall in the southwestern United States. *Water Resour. Res.* 15, 1701–1711. <https://doi.org/10.1029/WR015i006p01701>.
- Papalexiou, S.M., Koutsoyiannis, D., Montanari, A., 2011. Can a simple stochastic model generate rich patterns of rainfall events? *J. Hydrol.* 411, 279–289. <https://doi.org/10.1016/j.jhydrol.2011.10.008>.
- Peleg, N., Morin, E., 2014. Stochastic convective rain-field simulation using a high-resolution synoptically conditioned weather generator (HiReS-WG). *Water Resour. Res.* 50, 1–16. <https://doi.org/10.1002/2013WR014836>.
- Peleg, N., Morin, E., 2012. Convective rain cells: radar-derived spatiotemporal characteristics and synoptic patterns over the eastern Mediterranean. *J. Geophys. Res. Atmos.* 117, 1–17. <https://doi.org/10.1029/2011JD017353>.
- Racsko, P., Szeidl, L., Semenov, M., 1991. A serial approach to local stochastic weather models. *Ecol. Modell.* 57, 27–41. [https://doi.org/10.1016/0304-3800\(91\)90053-4](https://doi.org/10.1016/0304-3800(91)90053-4).
- Rebora, N., Ferraris, L., von Hardenberg, J., Provenzale, A., 2006. RainFARM: rainfall downscaling by a filtered autoregressive model. *J. Hydrometeorol.* 7, 724–738. <https://doi.org/10.1175/JHM517.1>.
- Renard, K.G., Lane, L.J., Simanton, J.R., Emmerich, W.E., Stone, J.J., Wetz, M.A., Goodrich, D.C., Yakowitz, D.S., 1993. Agricultural impacts in an arid environment: Walnut Gulch studies. *Hydrol. Sci. Technol.* 9, 145–190.
- Richardson, C.W., 1981. Stochastic simulation of daily precipitation, temperature, and solar radiation. *Water Resour. Res.* 17, 182–190. <https://doi.org/10.1029/WR017i001p00182>.
- Schuermans, J.M., Bierkens, M.F.P., 2006. Effect of spatial distribution of daily rainfall on interior catchment response of a distributed hydrological model. *Hydrol. Earth Syst. Sci. Discuss.* 3, 2175–2208. <https://doi.org/10.5194/hessd-3-2175-2006>.
- Serinaldi, F., 2009. A multisite daily rainfall generator driven by bivariate copula-based mixed distributions. *J. Geophys. Res. Atmos.* 114, 1–13. <https://doi.org/10.1029/2008JD011258>.
- Shuttleworth, W.J., 2012. *Terrestrial Hydrometeorology* Wiley-Blackwell ISBN-10: 0470659378.
- Stillman, S., Zeng, X., Shuttleworth, W.J., Goodrich, D.C., Unkrich, C.L., Zreda, M., 2013. Spatiotemporal variability of summer precipitation in southeastern Arizona. *J. Hydrometeorol.* 14, 1944–1951. <https://doi.org/10.1175/JHM-D-13-017.1>.
- Syed, K.H., Goodrich, D.C., Myers, D.E., Sorooshian, S., 2003. Spatial characteristics of thunderstorm rainfall fields and their relation to runoff. *J. Hydrol.* 271, 1–21. [https://doi.org/10.1016/S0022-1694\(02\)00311-6](https://doi.org/10.1016/S0022-1694(02)00311-6).
- Valdes, J.B., Rodriguez-Iturbe, I., Gupta, V.K., 1985. Approximations of temporal rainfall from a multidimensional model. *Water Resour. Res.* 21, 1259–1270. <https://doi.org/10.1029/WR021i008p01259>.
- Verdin, A., Rajagopalan, B., Kleiber, W., Katz, R.W., 2015. Coupled stochastic weather generation using spatial and generalized linear models. *Stoch. Environ. Res. Risk Assess.* 29, 347–356. <https://doi.org/10.1007/s00477-014-0911-6>.
- Verdin, A., Rajagopalan, B., Kleiber, W., Podestá, G., Bert, F., 2018. A conditional stochastic weather generator for seasonal to multi-decadal simulations. *J. Hydrol.* 556, 835–846. <https://doi.org/10.1016/j.jhydrol.2015.12.036>.
- von Hardenberg, J., Ferraris, L., Provenzale, A., 2003. The shape of convective rain cells. *Geophys. Res. Lett.* 30, 1–4. <https://doi.org/10.1029/2003GL018539>.
- Wilks, D.S., 1999. Simultaneous stochastic simulation of daily precipitation, temperature and solar radiation at multiple sites in complex terrain. *Agric. For. Meteorol.* 96, 85–101. [https://doi.org/10.1016/S0168-1923\(99\)00037-4](https://doi.org/10.1016/S0168-1923(99)00037-4).
- Wilks, D.S., 1998. Multisite generalization of a daily stochastic precipitation generation model. *J. Hydrol.* 210, 178–191. [https://doi.org/10.1016/S0022-1694\(98\)00186-3](https://doi.org/10.1016/S0022-1694(98)00186-3).
- Wilks, D.S., Wilby, R.L., 1999. The weather generation game: a review of stochastic weather models. *Prog. Phys. Geogr.* 23, 329–357. <https://doi.org/10.1191/030913399666525256>.
- Wischmeier, W.H., Smith, D.D., 1978. *Predicting Rainfall Erosion Losses: A Guide to Conservation Planning*. Dept. of Agriculture, Science and Education Administration Agriculture handbook, No. 537.